HHS Public Access

Author manuscript

Exp Cell Res. Author manuscript; available in PMC 2017 August 01.

Published in final edited form as:

Exp Cell Res. 2016 August 1; 346(1): 17–29. doi:10.1016/j.yexcr.2016.06.002.

Collective Epithelial Cell Sheet Adhesion and Migration on Polyelectrolyte Multilayers with Uniform and Gradients of Compliance

Jessica S. Martinez[a], **Joseph B. Schlenoff**[b], and **Thomas C. S. Keller III**[a,*]

Department of Biological Science and Department of Chemistry and Biochemistry, Florida State University, Tallahassee, Florida 32306

Abstract

Polyelectrolyte multilayers (PEMUs) are tunable thin films that could serve as coatings for biomedical implants. PEMUs built layer by layer with the polyanion poly(acrylic acid) (PAA) modified with a photosensitive 4-(2-hydroxyethoxy) benzophenone (PAABp) group and the polycation poly(allylamine hydrochloride) (PAH) are mechanically tunable by UV irradiation, which forms covalent bonds between the layers and increases PEMU stiffness. PAH-terminated PEMUs (PAH-PEMUs) that were uncrosslinked, UV-crosslinked to a uniform stiffness, or UV-crosslinked with an edge mask or through a neutral density optical gradient filter to form continuous compliance gradients were used to investigate how differences in PEMU stiffness affect the adhesion and migration of epithelial cell sheets from scales of the fish Poecilia sphenops (Black Molly) and Carassius auratus (Comet Goldfish). During the progressive collective cell migration, the edge cells (also known as ‘leader’ cells) in the sheets on softer uncrosslinked PEMUs and less crosslinked regions of the gradient formed more actin filaments and vinculin-containing adherens junctions and focal adhesions than formed in the sheet cells on stiffer PEMUs or glass. During sheet migration, the ratio of edge cell to internal cell (also known as ‘follower’ cells) motilities were greater on the softer PEMUs than on the stiffer PEMUs or glass, causing tension to develop across the sheet and periods of retraction, during which the edge cells lost adhesion to the substrate and regions of the sheet retracted toward the more adherent internal cell region. These retraction events were inhibited by the myosin II inhibitor Blebbistatin, which reduced the motility velocity ratios to those for sheets on the stiffer PEMUs. Blebbistatin also caused disassembly of actin filaments, reorganization of focal adhesions, increased cell spreading at the leading edge, as well as loss of edge cell-cell connections in epithelial cell sheets on all surfaces. Interestingly, cells throughout the interior region of the sheets on uncrosslinked PEMUs retained their actin and vinculin organization at adherens junctions after treatment with Blebbistatin. Like Blebbistatin, a Rho-kinase (ROCK) inhibitor, Y27632, promoted loss of cell-cell connections between edge cells, whereas a Rac1 inhibitor, NSC23766, primarily altered the

*To whom correspondence should be addressed. tkeller@bio.fsu.edu.

[a]Department of Biological Science.

[b]Department of Chemistry and Biochemistry.

lamellipodial protrusion in edge cells. Compliance gradient PAH-PEMUs promoted durotaxis of the cell sheets but not of individual keratocytes, demonstrating durotaxis, like plithotaxis, is an emergent property of cell sheet organization.

Graphical abstract

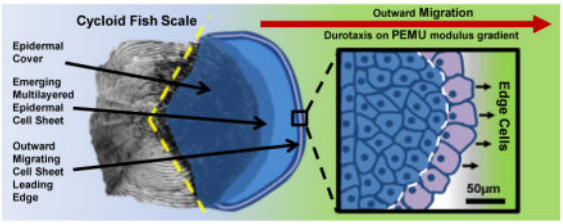

Keywords

Polyelectrolyte Multilayer (PEMU); Collective Cell Migration; Durotaxis; Poly(acrylic acid) (PAA); Poly(allylamine hydrochloride) (PAH); Myosin II; Modulus Gradient; Photocrosslinking

1. Introduction

Collective cell migration is crucial for normal tissue development and wound healing. Injury to skin, for example, triggers activation of various cells that release cytokines, remodel ECM, sprout blood vessels, and close the wound through epithelial cell sheet migration. [1] As epithelial cell sheets migrate to close the wound, unified contractile forces within the sheet help pull the skin tissue together. [1–3] Cells in these migrating multilayer sheets remain connected to each other through cadherin-containing cell-cell adhesions, which are stabilized by the cortical actin cytoskeleton and intermediate filaments. The interconnectedness of the cells and their traction as they move along the underlying substratum maintain robust mechanical tension throughout the migrating epithelial cell sheet. [2–3]

Cells can sense a variety of cues from their microenvironment, including surface modulus (stiffness), and respond to changes in microenvironment stiffness, stress, and elasticity by remodeling their cytoskeleton [4] and altering their morphology, substrate adhesion, and migration [5–8]. Some individual cells migrate directionally along a modulus gradient through a process known as durotaxis. [9–13]

Cells migrating collectively as a sheet through a process known as plithotaxis and cells migrating independently share certain characteristics but differ in their ability to affect each other mechanically and through signaling. Plithotaxis, an emergent property of cell sheets, requires coordination of cell motility that subjects individual cells within the collective cell sheet to additional regulation and restraints that control cell morphology and motility guidance [2–3, 14–15]; forces transmitted across cell-cell junctions direct individual cells to migrate along the local orientation of maximal principal stress, or equivalently, minimal intercellular shear stress. [16] Edge cell formation of robust vinculin-containing focal adhesions in highly active lamellipodia, in which actin filament turnover is controlled by

Rac-dependent signaling pathways, contributes to the traction at the sheet leading edge and development of tension across the sheet that is necessary for plithotaxis. [2–3, 17–20] Myosin II-dependent force production, controlled by Rho-dependent processes, maintains tensile forces on the focal adhesions in cells and across sheet cell-cell junctions. [21–24] Focal adhesions and stress fibers are components of mechanotransduction signaling pathways that enable a cell to sense physical cues from its environment such as surface modulus (stiffness) and intracellular shear stress. [8, 25–32] During collective cell plithotaxis, intercellular response to extracellular signals is processed by edge cells and subsequently transmitted via chemical or mechanical signaling to internal cells, eliciting a larger and more expanded response throughout the collective sheet. Polarity is established in both individual edge cells and through the collective mass, forming a front and back end in the migrating cell sheet. Guidance signals distributed throughout the sheet regulate individual cell responses. [3] Collectively, sheet cells can sample cues from a larger area than can a single cell. [2–3] Because every cell of the collective provides input regarding environmental guidance cues, the sheet responds as a coordinated unit to global guidance cues rather than to more local differences in cues. [2]

Epithelial tissue isolated from fish scales provides an excellent model cell system for studying migration of individual cells and epithelial cell sheets of the type observed during wound healing. [20, 33–34] In this study, we used primary explants of epithelial cell sheets associated with scales of the fish Poecilia sphenops (Black Molly) and Carassius auratus (Comet Goldfish) to investigate collective cell interaction with polyelectrolyte multilayers (PEMUs).

PEMUs are thin film coatings built layer by layer with alternating pairs of polyelectrolytes (PEs). [35–36] Varying parameters such as the specific types of PE used, number of layers, and degree of layer crosslinking yields PEMUs with a wide variety of bulk chemical and physical properties. [35–43] Ability to tune PEMU properties to mimic aspects of natural cell microenvironments that affect cell behavior such as adhesion makes PEMUs potentially useful in biomedical applications. [44–46]

PEMUs used in this investigation were built with alternating layers of the polyanion PAA-PAABp [PAA (poly(acrylic acid)) modified with a photosensitive 4-(2-hydroxyethoxy) benzophenone (PAABp)], and the polycation PAH (poly(allylamine hydrochloride)). Photoactivation of the PAABp generates covalent crosslinks between the layers, increasing surface modulus. [47] Varying the time of crosslinking generates surfaces with varied uniform moduli. Photoactivation through an optical gradient mask generates modulus gradients. [47] Because only 5% of the PAA side groups were modified with the photosensitive benzophenone group, surface modulus manipulation by crosslinking has little effect on net surface charge. This investigation is the first to characterize fish scale cell sheet behavior on PEMUs and demonstrates sheet durotaxis on a compliance gradient and the importance of myosin II activity on sheet integrity and motility.

2. Materials and methods

2.1 Polyelectrolytes and Reagents

Poly(acrylic acid) (PAA, molar mass 100,000 g mol^{-1}) and poly(allylamine hydrochloride) (PAH, molar mass 56,000 g mol^{-1}) from Sigma-Aldrich, and poly(ethyleneimine) (PEI, molar mass 70,000 g mol^{-1}) from Polysciences, Inc. (Warrington, PA) were used as received. PAA grafted with photosensitive benzophenone (5 mol%) was synthesized as described previously. [47] Unless noted otherwise, all other reagents were used as received from Sigma-Aldrich. For myosin II, Rho kinase (ROCK), and Rac1 inhibition, cell sheets were treated with low and high concentrations of inhibitors as follows: 5 μM and 50 μM Blebbistatin (myosin II inhibitor), 1 μM and 50 μM of Y27632 (Rho Kinase [ROCK] inhibitor), and 5 μM and 50 μM NSC23766 (Rac1 inhibitor). Cell sheets were observed for 1 hour before treatment and for 3 hours after treatment.

2.2 Polyelectrolyte Structures

The PAABp benzophenone side group (m) is 5% of the total monomer units (n). (n=1; m=0.05; n−m=0.95).

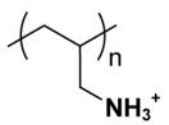

PAH

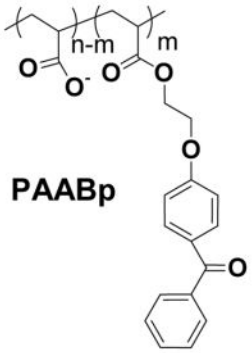

PAABp

2.3 Polyelectrolyte Multilayer Preparation

The 31-layer PAH-terminated PEI(PAABp/PAH)$_{15}$ PEMUs used in this investigation were built using 10 mM (with respect to the repeat unit) PE solutions made in 0.15 M NaCl, 25 mM Tris-HCl, pH 7.4, as described previously. [47] The PEMUs were built on Fisherbrand Cover Glass No. 1 (Fisher Scientific) 22 × 22 × 0.17 mm coverslips for uniform modulus and steep modulus gradient assays, and on 50 × 22 × 0.17 mm coverslips for shallow modulus gradient assays. Prior to PEMU coating, the glass coverslips were cleaned by soaking in 70% ethanol overnight, rinsed extensively with H_2O, dried with a stream of N_2, and exposed to an air plasma for 1 min. All surfaces were first primed with a layer of PEI by dipping into PEI solution for 30 min and rinsing with water. This initial PEI layer promoted a more uniform coating by subsequent PE layers. The remainder of the PEMU was built layer by layer with the aid of a robot (StratoSequence V, nanoStrata Inc., Tallahassee, FL). The PEI-coated surfaces were mounted in the robot on a shaft that rotated at 300 rpm for 15 cycles of dipping in alternating baths of PAABp and PAH for 5 min each, with three 1-min water rinsing steps between each PE bath. Before use in cell culture, the PEMU-coated coverslips were incubated overnight in 0.15 M NaCl, 25 mM Tris-HCl, pH 7.4. All PE

solutions used for building the cell culture PEMUs contained 0.02 wt% sodium azide to prevent microbial contamination. PEMUs were handled and stored using sterile laboratory practices. Microbial contamination of polyelectrolyte solutions lacking sodium azide was rare, and its inclusion was only precautionary and unnecessary if PEMUs were handled following sterile practices. Azide was rinsed out of PEMUs in the final rinsing step. No significant differences were found by AFM spectroscopy or cell culture analysis in PEMUs built with or without sodium azide (data not shown).

2.4 Photocrosslinking

For photocrosslinking, PEI(PAABp/PAH)$_{15}$ PEMUs were dried after the final water rinse and irradiated in a 12.7 × 30.5 × 25.4 cm CL-1000 Model 254 nm UV box (Ultra-Violet Products Ltd., Upland, CA) equipped with five 8 W 200–280 nm wavelength UV lamps and a calibration photodiode. The PEMUs were placed at the center of the box where the UV intensity at the surface level was 4.9 mW cm^{-2}. Irradiating a PEMU transforms the benzophenone to a biradical (ketyl radical), which either can form a crosslinking covalent bond with PAH or return to ground state by phosphorescence. [47]

Shallow modulus gradients in the PEI(PAABp/PAH)$_{15}$ PEMUs on coverslips were formed by irradiating for 200 min through a rectangular continuously variable neutral density gradient filter composed of a UV-fused silica glass substrate with a metallic Inconel gradient surface coating (NDL-10C-2, Thorlabs, Newton, NJ). The coated part of the filter is 45 mm long, over which the optical density along the coating varies from 0.04 to 2. Steeper modulus gradients were generated by masking half the multilayer with an opaque black shield and exposing the other half to UV irradiation for 100 min. The position of the mask edge was marked for future reference.

2.5 Primary Fish Epithelial Tissue Explant

Poecilia sphenops (Black Molly) and Carassius auratus (Comet Goldfish) were obtained from a local pet store and euthanized on arrival in the lab in accordance with approved Institutional Animal Care and Use Committee (IACUC) protocols for tropical and non-tropical fish. Both fish types were euthanized by immersion in MS-222 (tricaine) at 2 g L^{-1} in freshly drawn well water. The fish carcass was kept ice cold and washed periodically with 1 mL of cold sterile phosphate-buffered saline (PBS, pH 7.4) containing 10 μg mL^{-1} gentamicin (Gibco Gentamicin Reagent Solution, Invitrogen) and an antibiotic-antimycotic supplement with a final concentration of 100 units mL^{-1} penicillin G, 100 μg mL^{-1} streptomycin, and 0.25 μg mL^{-1} amphotericin (Gibco Antibiotic-Antimycotic, Invitrogen) during removal of scales.

Fish scales were plucked from the fish and placed onto the PEMU and uncoated glass surfaces. The side of the fish scale originally in contact with the fish epidermis was placed down onto the surface, ensuring direct contact between the primary fish epithelial tissue explants and the substrate. After 2 minutes at room temperature, the scale-surface preparation was gently immersed in sterile PBS containing the antibiotic-antimycotic supplements for five minutes. The PBS was gently aspirated and replaced with RPMI 1640 culture media (cat. No. A10491, Gibco, Invitrogen) supplemented with 30% fetal bovine

serum (HyClone Standard Bovine Serum, Thermo Scientific), 10 μg mL^{-1} gentamicin (Gibco Gentamicin Reagent Solution, Invitrogen), 100 units mL^{-1} penicillin G, 100 μg mL^{-1} streptomycin, and 0.25 μg mL^{-1} amphotericin. 150 μL of supplemented culture media was used for every 484 mm^{-2} of substrate area. A clean coverslip was placed on top, sandwiching the fish-scale in supplemented culture media. This coverslip-surface sandwich was placed in a 100 mm plastic petri dish that was glued onto a covered 150 mm plastic petri dish filled with H_2O to create a 'humidification chamber'. This 'humidification chamber' was kept in the dark at room temperature (25 °C) for 24 hours. Every 24 hours, the fish scale containing surfaces were washed with antibiotic-antimicrobial containing sterile PBS for five minutes, re-sandwiched with fresh supplemented culture media, and placed back into the 'humidification chamber'.

The primary fish epithelial tissue emerged from each scale after 24 hours and migrated outward. These primary cell sheet explants continued to migrate away from their scale of origin while remaining attached to the scale. Experimental observations in this study were conducted after 24 hours of establishing the cultured explant. Cell sheets were observed up to 72 hours. No significant differences in adhesion and motility were observed for sheets first emerging from either type of fish scale at different time points. The type of fish scale used for each figure is indicated in the figure legend.

2.6 Time Lapse and Live Cell Imaging

A Nikon Ti-E inverted microscope equipped with a Nikon Intensilight C-HGFI illuminator and a Photometrics Cool Snap HQ2 camera (Photometrics) was used to obtain differential interference contrast (DIC) images of fixed cells and to record live cell activity. Phase contrast images were captured using a Nikon TS100 microscope equipped with a Nikon Digital Sight DS-Ri1 digital camera. Fixed cell images and live cell recordings were analyzed and processed using NIS-Elements Advanced Research (Nikon), ImageJ (NIH), and Photoshop (Adobe) software.

Kymographs were created using Nikon imaging software

During live cell analysis (see Imaging) cells were maintained under the microscope at 27 °C and 40% relative humidity in a LiveCell™ Chamber (Pathology Devices, Westminster, MD). To facilitate DIC imaging of live cells on PEMUs, a 22 × 22 × 0.17 mm coverslip (uncoated or coated with PEMUs of uniform modulus or PEMUs containing a steep or shallow modulus gradient) was attached to the bottom opening of a 35 mm tissue culture dish (created by drilling into the bottom of the plastic culture dish with a variable drill press fitted with a smooth-finish wood bit: ¾″ diameter McMaster-Carr, Cleveland, OH) using glue (Gorilla Glue, Inc.). The drilled culture dishes were sterilized with 70% ethanol and washed extensively with sterile PBS before attaching the PEMU-coated and uncoated coverslips. The glue was allowed to cure for at least 24 hours, after which the 'windowed' culture dishes were washed extensively with PBS to remove any remaining particulates. Wet mounts of PEMUs containing a shallow modulus gradient were created on glass slides (76.2 × 24.5 × 1 mm) using Vaseline to seal the edges of the coated coverslips. These wet mounts can be maintained for 24 hours and were used for live cell observations of cell sheets on PEMUs containing shallow modulus gradients.

2.8 Fluorescent Localization of Vinculin and Actin

Fish scale containing “sandwiched’ surfaces were placed on ice for five minutes before fixing with freshly prepared 3.7% paraformaldehyde (powder, molecular-biology grade paraformaldehyde, Fisher Scientific) in PBS for 10 minutes at room temperature. The fixative solution was removed and the cell sheet containing scales were washed PBS three times for 5 min each, treated with 0.2% Triton X-100-PBS for 10 minutes followed by three 5 minute rinses with 0.05% Triton X-100-PBS, and blocked with 1% bovine serum albumin prepared in 0.05% Triton X-100-PBS for 30 minutes, all at room temperature. After blocking, the staining protocol described previously [48] was followed using an anti-vinculin mouse monoclonal primary antibody (Sigma-Aldrich, clone VIN-11-5, 1:200 dilution), Alexa Fluor 568 and 488 phalloidins (Invitrogen, 1:100 dilution), and Alexa Fluor 568 and 488 goat anti-mouse IgG secondary antibodies (Invitrogen, 1:800 dilution). All antibodies were prepared in 1% goat serum containing 0.05% Triton X-100-PBS buffer. Phalloidin was prepared in 1% bovine serum albumin containing 0.05% Triton X-100-PBS buffer. Additionally, preparations also were stained with DAPI (Invitrogen) prepared at a final concentration of 1 μg mL^{-1} in PBS to visualize cell nuclei. All stained surfaces were mounted with freshly prepared Gelvatol (0.13% v/v 1.5 M Tris pH 8.8, 0.21% v/v glycerol, 0.11% w/v poly(vinyl alcohol) molar mass 30,000–70,000 g mol^{-1}, 0.02% w/v sodium azide, stirred on low heat for 4 hours) onto microscope slides and allowed to cure for 24 hours. Edges were sealed with clear nail polish and stored in the dark at room temperature.

Corrected total cell fluorescence (CTCF) was used to quantify actin filament and vinculin fluorescence in individual cells under various conditions. CTCF was calculated using ImageJ (NIH) by drawing a fixed size outline along the periphery of each edge cell and internal cell using differential interference contrast (DIC) images as a reference to analyze area where focal adhesions and cell-cell contacts were located. The area of the cell outline, the integrated fluorescence density, and mean gray value for each cell (n =20) as well as the localized background fluorescence was measured. CTCF was calculated as integrated density – (area of selected outline × mean gray value of background readings).

2.9 Migration Plot of Cell Sheets on PEMUs

Motility of cell sheets was recorded at a rate of one image every 30 sec (120 images per h) for up to 3 h. The ImageJ Manual Tracking plugin was used to track the (x, y) coordinates of each cell nucleus over time, and Excel was used to generate the migration plot (the real position of the nuclei (x, y) coordinate with time) of migrating sheet cells. Migration of five edge cells (cells along the leading edge of the cell sheet) and five internal cell nuclei (internal cells along the cell sheet) were compared. Wind rose plots were constructed as previously described. [49]

3. Results

3.1 Collective Cell Migration of Primary Fish Scale Epidermal Tissue Explants - Plithotaxis

A multilayered epidermal tissue covers the dorsal posterior region of cycloid fish scales (Fig. 1). When a scale is explanted from a Poecilia sphenops (Black Molly) or a Carassius auratus (Comet Goldfish) and placed fish body side down on a suitable substrate, the epidermal

tissue sheet initiates a wounding response, in which the epidermis migrates as a collective sheet out from the scale onto the underlying substrate (Fig. 1). The sheet migrates with a coherent leading front of ‘edge’ cells (defined as cells at the leading edge of sheets with at least one side not in contact with another cell, also see Supporting Information Fig. S1), which form robust stress fibers and focal adhesions in their prominent lamellipodia. Intercellular junctions connect the edge cells to each other and to the following interconnected ‘internal’ cells (Fig. 1E).

3.2 Epidermal Sheet Integrity and Plithotaxis is Myosin II Dependent

Treating cell sheets emerging from explanted scales on uncoated coverslips for 3 hours with the myosin II inhibitor Blebbistatin or the Rho kinase inhibitor Y27632, which also inhibits myosin II activity, caused loss of intercellular junctions (Fig. 2). Leading edge cells dissociated from the sheet and migrated across the surface independently in random directions, leaving behind a new and far less coherent edge on the migrating cell sheet. Over time, cells in the new edge similarly dissociated from the cell sheet, and breaking of weakened connections between internal cells formed holes in the sheets. The higher (50 μm) Blebbistatin and Y27632 concentrations caused more rapid onset of effects and more extensive dissociation of edge cells from the cell sheets. In addition, both treatments caused a decrease in cell sheet directional migration, and disconnecting cells exhibited impaired motility and abnormal morphology. The disconnecting cells became overstretched, especially around holes formed.

Epithelial cell sheets treated with the Rac1 inhibitor NSC23766 remained mostly intact, but progressive sheet migration was impaired (Fig. 2) and the edge cell lamellipodia ruffling pattern was less uniform than in the no treatment controls (Fig. 3). Individual keratocytes migrating away from the sheet also had developed defective lamellipodia. As with the myosin II inhibitors, the higher Rac1 inhibitor concentration caused more rapid onset of effects.

3.3 Cell Sheets migrating on PAH-PEMUs – Effects of Myosin II inhibition

Uncrosslinked PAH-PEMUs have a positive surface charge and a uniform modulus (~38 MPa) that is more compliant than glass. [49] Epidermal cell sheets migrated from explanted scales on PAH-PEMUs as fast as or faster than did sheets on uncoated glass (Fig. 4). Tracking the velocities of edge and internal cell migrations revealed edge cell:internal cell velocity ratios of approximately 1.2 for sheets on uncoated glass and close to 1.5 for sheets on PAH-PEMUs. This suggests that sheets on PAH-PEMUs develop a greater tension across the sheet than do the sheets on uncoated glass. Consistent with this, treatment with Blebbistatin had little no overall inhibition on the velocities of the edge and internal cells in sheets on glass, despite the effects on sheet integrity, but decreased the velocity of the edge cells relative to that of the internal cells on PAH-PEMUs.

A greater degree of tension within the sheets migrating on the uniform modulus PAH-PEMUs than on uncoated glass also was apparent in sheets that were immunofluorescently stained for the actin filaments and the junctional protein vinculin (Fig. 5A–D). Compared to the cells in sheets on glass, cells in sheets on PAH-PEMUs were more elongated (Fig. 5E–

G) and had a more robust actin network and greater localization of vinculin (Figure 5H–I). These indicators of cellular tension decreased after treatment with the myosin II inhibitor Blebbistatin, but remained greater than in sheets on uncoated coverslips (Fig. 5E–G). When treated with 5 μM Blebbistatin, the average major: minor axis ratio decreased significantly as in the cells in sheets on uncoated coverslips, but the cell area of the Blebbistatin-treated cells increased to a level significantly greater in cells on PAH-PEMUs than on the uncoated coverslips.

3.4 Collective Cell Sheet Durotaxis along Shallow and Steep PAH-PEMU Modulus Gradients

PAH-PEMUs were photocrosslinked with no mask, with an edge mask to generate steep modulus gradients (35–120 MPa; ~1.5 mm long; ~55 MPa mm^{-1}), and through an optical density mask to generate shallow modulus gradients (35–120 MPa; ~15 mm long; ~5.5 MPa mm^{-1}) [49]. As it migrates out, the length of a migrating cell sheet can reach 2 mm in length, long enough to span the entire steep modulus gradient and to span a difference of 11 MPa on the shallow gradient.

When explanted scales were placed near the middle of a shallow gradient (~90 MPa) and positioned so that the migrating epidermal cell sheets were oriented toward the stiffer end of the gradient, the sheet migration proceeded toward the stiffer end of the gradient (Fig. 6A). Both the edge cells and the internal cells in sheets on the PAH-PEMU shallow modulus gradients migrated faster than equivalent cells in sheets on uniform modulus uncrosslinked PAH-PEMUs (compare Fig. 6C to Fig. 4B) and the edge cell:internal cell velocity ratio also was slightly higher (compare Fig. 6D to Fig. 4C). Morphologies of cells in the sheets on shallow gradients showed linear indications of stress in regions of the sheets migrating along the gradient (Fig 6A, enlargements). Accordingly, cell sheets on the shallow modulus gradients were unable to maintain a continuous progressive migration and underwent episodic retraction events. During each retraction, the sheet leading edge lost adhesion to the surface and retracted back toward a boundary of a nonretracting internal cell mass.

Sheets also retracted on uniform modulus PAH-PEMUs, but the retractions were more localized along the leading edge and the distances on uncrosslinked uniform modulus PAH-PEMUs were significantly shorter than on the gradients (Fig 6B). In addition, the sheets resumed forward migration much more quickly than after the major retractions on the shallow gradients. Migration behaviors of sheets on maximally crosslinked PAH-PEMUs of uniform stiff modulus and on the stiffest region of the shallow gradient were comparable to those on uncoated coverslips and did not exhibit retraction events (not shown). Kymographs show that on uncoated coverslips untreated sheets migrate forward with no retraction and that Blebbistatin treatment impairs forward migration. Sheets on PEMUs that are untreated undergo the retraction, which is eliminated by Blebbistatin treatment, allowing forward migration without impairment as seen with sheets on uncoated surfaces (Fig 7).

A migration plot analysis of 4 edge cells and 6 internal cells in a sheet on an uncoated glass coverslip confirmed each of the individual cells in the migrating sheet moved linearly, plithotaxing away from the fish scale (Fig. 8B). In contrast, when scales were oriented on PAH-PEMU shallow modulus gradient so that direction of sheet emergence was parallel to

the gradient but oriented toward the softer end of the gradient, each of the 4 edge and 6 internal cells deviated from typical linear migration and turned perpendicular to the gradient or even eventually moved toward the stiffer end of the gradient (Fig. 8C). One side region of the cell sheet on the shallow gradient (Fig. 8A, lower region of the sheet) established a more robust lamellipodial front, and migration of both the edge and internal cells curved the migration of the sheet away from the decreasing substrate modulus and toward the increasing substrate modulus. Plithotaxis was conserved in these sheets as they durotaxed in response to the modulus gradient. Intriguingly, cells within sheets migrating across a steep modulus gradient extensively elongated and oriented toward the stiffest end of the gradient without completely disrupting the sheet (Fig. 9). Cells that previously had migrated across the steep gradient region onto the stiffest region (Fig 9B) reestablished morphologies similar to those of cells on uniform modulus PAH-PEMUs (Fig 9A). These results demonstrate that the epidermal sheets can accommodate levels of shear tension that significantly elongate cells without losing sheet integrity.

Responses of cells in sheets on both the shallow and stiff PEMU modulus gradients raised the question of whether individual cells also respond to the gradients. Wind rose plots of 10 migrating keratocyte cells that had broken off sheets showed no uniform directed migration or durotaxis on an uncoated coverslip or on PAH-PEMUs with uniform modulus or shallow or steep modulus gradients (Fig. 10).

4. Discussion

Collective cell migration is poorly understood. PEMUs provide a novel tool for modulating cell sheet adhesion and migration responses to differences in substrate modulus. Our previous studies have shown that the 31-layer PEMUs used in this investigation are thick enough to establish a modulus that is independent of the underlying glass modulus. [50] Manipulation of this PEMU surface modulus by photocrosslinking has minimal effect on the PEMU surface charge, because only 5% of the PAA side groups are modified with the photosensitive benzophenone groups that form the PEMU crosslinks. In our previous studies, we demonstrated the biocompatibility of PAH/PAA PEMUs and analyzed the behavior of single cells on similar PAH-PEMUs containing steep and shallow modulus gradients. [49, 51]

Live cell image analysis in this investigation revealed that both edge and internal cells migrated significantly faster on uniform modulus and shallow gradient modulus PAH-PEMUs than on uncoated control coverslips. Additionally, comparison of the average velocity ratios between edge and internal cells of approximately 1.2 (coverslips), 1.5 (uniform modulus PAH-PEMUs), and 1.7 (PAH-PEMUs containing a shallow modulus gradient) revealed that edge cells migrated significantly faster than internal cells in sheets on PAH-PEMUs.

Greater differences in edge and internal cell migration velocities suggest that sheets on the PAH-PEMUs, especially on the modulus gradient, are subject to greater internal tension than are sheets migrating on glass. Four properties of the sheets on modulus gradients provide evidence they have greater internal tension. First, sheet cells on PAH-PEMUs assemble more

actin filaments and develop more robust vinculin-containing cell-cell junctions and focal adhesions. Second, sheets on PAH-PEMU shallow gradients undergo episodic periods of retraction, during which a region containing edge and internal cells at the front of a migrating sheet retracts back about 150 μm (roughly 10 cell lengths) before migrating out again. These retraction events are similar to those reported for primary zebrafish keratocyte collective cell migration on surfaces in the presences of RGD peptide, which inhibits integrin-mediated adhesion. [20] Differential substrate adhesion has been shown to be a main component of mechanosensing, durotaxis, and directional migration [53] and likely is a major contributor to the retraction behavior of the sheets on the different PEMU substrates. Third, individual cells in sheets exhibit morphologies indicative of increased tension (as in Figs. 5 and 6). Immediately before cell sheet retraction, stress lines in the sheets often are visible (as in Fig. 6). Fourth, cells in sheets directly over the PAH-PEMU region of steep modulus gradient are highly elongated, whereas cells on the uniform softer and stiffer modulus ends are not. In contrast, sheets on uniform modulus PAH-PEMUs or on the stiffer regions of the shallow gradient underwent minimal or no retraction events and their migration behaviors were similar to those on uncoated coverslips.

Contributions of myosin II force production and Rac- and Rho-dependent processes to sheet plithotaxis and durotaxis were investigated with inhibitors. Both direct and indirect myosin II inhibitors, Blebbistatin and ROCK inhibitor Y27632, caused a progressive dissociation of cells from the sheet edge. Low concentrations of Blebbistatin also decreased retractions and promoted sustained migration of sheets on PAH-PEMUs by decreasing the average velocity of the edge cells and lowering the velocity ratio between edge and internal cells to 1.2. When edge cells dissociated and migrated away from the sheet in Blebbistatin, they left a new edge of what previously were internal cells, which also dissociated and migrated away from the sheet over time. In dissociating from the sheet, Blebbistatin-treated cells exhibited impaired motility compared to untreated keratocytes; many became highly elongated with an extended cell body dragging behind. Collectively, these results indicate that myosin II activity is a critical contributor to the overall mechanisms of both single cell and collective cell migration by helping to coordinate activities at the leading and lagging ends of cells and stabilizing cell-cell junctions in cell sheets.

In contrast, treatment with Rac1 inhibitor NSC23766 caused a decrease in edge cell lamellipodia ruffling coupled to a decrease in sheet migration velocity but no extensive cell dissociation from other cells within the sheet or from the sheet. This confirms a role for Rac and edge cell lamellipodia formation in forward sheet migration not in maintaining sheet integrity.

The intriguing question of whether cell sheets can durotax was addressed by analysis of sheet migration on PAH-PEMU shallow modulus gradients. When cell sheets were oriented on PAH-PEMU shallow modulus gradients toward the softer end, the migration trajectory of the collective sheet and cells within the sheet deviated from linear forward migration exhibited by sheets on glass and uniform modulus PAH-PEMUs and reoriented toward the gradient stiffer end. On the shallow modulus gradient, edge cells in one region of the cell sheet on the highest modulus established robust and highly active lamellipodia and curved the entire cell sheet migration away from the softer modulus and toward the higher modulus.

The sheet reorientation proceeded without changing relative positions of individual cells in the sheet. Evidence from other investigations has indicated tensional gradients across an individual cell within the sheet is established by traction forces on the underlying substrate and the transmission stress of cell-cell contacts. [54] These mechanical cues polarize both individual cells within the sheet and the cell sheet as a whole. As a collective, cell sheets coordinate the tensional gradients of individual cells affecting both the local (at the individual cell level) and global (throughout the sheet) response to the mechanical stress. [55] Further demonstrating the critical role cell-cell contacts play in directing a collective migratory response in cell sheets, individual cells breaking off the sheets exhibit no durotaxis, indicating that durotaxis like plithotaxis is an emergent property of the cell sheets.

Supplementary Material

Refer to Web version on PubMed Central for supplementary material.

Acknowledgments

This work was supported by grants from the NIH (R01EB006158), National Science Foundation (DMR-0939850), and the Florida State University. We thank other members of the Schlenoff lab and Keller lab for helpful discussions and suggestions that improved the manuscript.

References

1. Eckes B, Nischt R, Krieg T. Cell-matrix interactions in dermal repair and scarring. Fibrogenesis & Tissue Repair. 2010; 3:4. [PubMed: 20222960]
2. Rorth P. Collective guidance of collective cell migration. Trends in Cell Biology. 2007; 17:575–579. [PubMed: 17996447]
3. Rorth P. Collective Cell Migration. Annual Review of Cell and Developmental Biology. 2009; 25:407–429.
4. Guilak F, Cohen DM, Estes BT, Gimble JM, Liedtke W, Chen CS. Control of Stem Cell Fate by Physical Interactions with the Extracellular Matrix. Cell Stem Cell. 2009; 5:17–26. [PubMed: 19570510]
5. Singer. FIBRONEXUS - TRANSMEMBRANE ASSOCIATION OF FIBRONECTIN-CONTAINING FIBERS AND BUNDLES OF 5 NM MICROFILAMENTS IN HAMSTER AND HUMAN-FIBROBLASTS. Cell. 1979; 16:675–685. [PubMed: 222466]
6. Dugina V, Fontao L, Chaponnier C, Vasiliev J, Gabbiani G. Focal adhesion features during myofibroblastic differentiation are controlled by intracellular and extracellular factors. Journal of Cell Science. 2001; 114:3285–3296. [PubMed: 11591817]
7. Hinz B, Gabbiani G. Mechanisms of force generation and transmission by myofibroblasts. Current Opinion in Biotechnology. 2003; 14:538–546. [PubMed: 14580586]
8. Vogel V. Mechanotransduction involving multimodular proteins: Converting force into biochemical signals. Annual Review of Biophysics and Biomolecular Structure. 2006; 35:459–488.
9. Isenberg BC, Di Milla PA, Walker M, Kim S, Wong JY. Vascular smooth muscle cell durotaxis depends on substrate stiffness gradient strength. Biophys J. 2009; 97:1313–1322. [PubMed: 19720019]
10. Lo CM, Wang HB, Dembo M, Wang YL. Cell movement is guided by the rigidity of the substrate. Biophys J. 2000; 79:144–152. [PubMed: 10866943]
11. Nemir S, Hayenga HN, West JL. PEGDA Hydrogels With Patterned Elasticity: Novel Tools for the Study of Cell Response to Substrate Rigidity. Biotechnology and Bioengineering. 2010; 105:636–644. [PubMed: 19816965]
12. Discher DE, Janmey P, Wang Y-l. Tissue Cells Feel and Respond to the Stiffness of Their Substrate. Science (Washington, DC, United States). 2005; 310:1139–1143.

13. Gray DS, Tien J, Chen CS. Repositioning of cells by mechanotaxis on surfaces with micropatterned Young's modulus. Journal of Biomedical Materials Research Part A. 2003; 66A: 605–614. [PubMed: 12918044]
14. Friedl P, Gilmour D. Collective cell migration in morphogenesis, regeneration and cancer. Nature Reviews Molecular Cell Biology. 2009; 10:445–457. [PubMed: 19546857]
15. Lee JM, Dedhar S, Kalluri R, Thompson EW. The epithelial-mesenchymal transition: new insights in signaling, development, and disease. Journal of Cell Biology. 2006; 172:973–981. [PubMed: 16567498]
16. Trepat X, Fredberg JJ. Plithotaxis and emergent dynamics in collective cellular migration. Trends in Cell Biology. 2011; 21:638–646. [PubMed: 21784638]
17. Burridge K, Wennerberg K. Rho and Rac take center stage. Cell. 2004; 116:167–179. [PubMed: 14744429]
18. Burton K, Park JH, Taylor DL. Keratocytes Generate Traction Forces in Two Phases. Mol Biol Cell. 1999; 10:3745–3769. [PubMed: 10564269]
19. Cortese B, Gigli G, Riehle M. Mechanical Gradient Cues for Guided Cell Motility and Control of Cell Behavior on Uniform Substrates. Advanced Functional Materials. 2009; 19:2961–2968.
20. Rapanan JL, Cooper KE, Leyva KJ, Hull EE. Collective cell migration of primary zebrafish keratocytes. Experimental Cell Research. 2014; 326:155–165. [PubMed: 24973510]
21. Mertz AF, Che YL, Banerjee S, Goldstein JM, Rosowski KA, Revilla SF, Niessen CM, Marchetti MC, Dufresne ER, Horsley V. Cadherin-based intercellular adhesions organize epithelial cell-matrix traction forces. Proceedings of the National Academy of Sciences of the United States of America. 2013; 110:842–847. [PubMed: 23277553]
22. Ng MR, Besser A, Danuser G, Brugge JS. Substrate stiffness regulates cadherin-dependent collective migration through myosin-II contractility. Journal of Cell Biology. 2012; 199:545–563. [PubMed: 23091067]
23. Theveneau E, Mayor R. Collective cell migration of epithelial and mesenchymal cells. Cellular and Molecular Life Sciences. 2013; 70:3481–3492. [PubMed: 23314710]
24. Omelchenko T, Vasiliev JM, Gelfand IM, Feder HH, Bonder EM. Rho-dependent formation of epithelial "leader" cells during wound healing. Proceedings of the National Academy of Sciences of the United States of America. 2003; 100:10788–10793. [PubMed: 12960404]
25. Asparuhova MB, Gelman L, Chiquet M. Role of the actin cytoskeleton in tuning cellular responses to external mechanical stress. Scandinavian Journal of Medicine & Science in Sports. 2009; 19:490–499. [PubMed: 19422655]
26. Vogel V, Sheetz M. Local force and geometry sensing regulate cell functions. Nat Rev Mol Cell Biol. 2006; 7:265–275. [PubMed: 16607289]
27. Liedert A, Kaspar D, Blakytny R, Claes L, Ignatius A. Signal transduction pathways involved in mechanotransduction in bone cells. Biochemical and Biophysical Research Communications. 2006; 349:1–5. [PubMed: 16930556]
28. Ingber DE. Cellular mechanotransduction: putting all the pieces together again. Faseb Journal. 2006; 20:811–827. [PubMed: 16675838]
29. Li S, Huang NF, Hsu S. Mechanotransduction in endothelial cell migration. Journal of Cellular Biochemistry. 2005; 96:1110–1126. [PubMed: 16167340]
30. Ingber DE. Tensegrity: The architectural basis of cellular mechanotransduction. Annual Review of Physiology. 1997; 59:575–599.
31. Leckband DE, le Duc Q, Wang N, de Rooij J. Mechanotransduction at cadherin-mediated adhesions. Current Opinion in Cell Biology. 2011; 23:523–530. [PubMed: 21890337]
32. Fournier MF, Sauser R, Ambrosi D, Meister JJ, Verkhovsky AB. Force transmission in migrating cells. Journal of Cell Biology. 2010; 188:287–297. [PubMed: 20100912]
33. Matsumoto R, Sugimoto M. Dermal matrix proteins initiate re-epithelialization but are not sufficient for coordinated epidermal outgrowth in a new fish skin culture model. Cell Tissue Res. 2007; 327:249–265. [PubMed: 17043792]
34. McDonald TM, Pascual AS, Uppalapati CK, Cooper KE, Leyva KJ, Hull EE. Zebrafish keratocyte explant cultures as a wound healing model system: Differential gene expression & morphological

changes support epithelial –mesenchymal transition. Experimental Cell Research. 2013; 319:1815–1827. [PubMed: 23588205]

35. Decher G. Fuzzy nanoassemblies: Toward layered polymeric multicomposites. Science. 1997; 277:1232–1237.
36. Schlenoff JB, Ly H, Li M. Charge and mass balance in polyelectrolyte multilayers. J Am Chem Soc. 1998; 120:7626–7634.
37. Dubas ST, Schlenoff JB. Factors controlling the growth of polyelectrolyte multilayers. Macromolecules. 1999; 32:8153–8160.
38. Dubas ST, Schlenoff JB. Factors controlling the growth of polyelectrolyte multilayers. Abstr Pap Am Chem S. 2000; 219:U532–U532.
39. Dubas ST, Schlenoff JB. Swelling and smoothing of polyelectrolyte multilayers by salt. Langmuir. 2001; 17:7725–7727.
40. Dubas ST, Schlenoff JB. Salt-controlled processing of thin films: Multilayers containing a weak polyacid. Abstr Pap Am Chem S. 2001; 221:U415–U415.
41. Dubas ST, Schlenoff JB. Polyelectrolyte multilayers containing a weak polyacid: Construction and deconstruction. Macromolecules. 2001; 34:3736–3740.
42. Decher G, Schlenoff JB. Multilayer Thin Films: Sequential Assembly of Nanocomposite Materials. 2003
43. Sui Z, Salloum D, Schlenoff JB. Effect of Molecular Weight on the Construction of Polyelectrolyte Multilayers: Stripping versus Sticking. Langmuir. 2003; 19:2491–2495.
44. Schneider A, Francius G, Obeid R, Schwinté P, Hemmerlé J, Frisch B, Schaaf P, Voegel J-C, Senger B, Picart C. Polyelectrolyte Multilayers with a Tunable Young's Modulus: Influence of Film Stiffness on Cell Adhesion. Langmuir. 2006; 22:1193–1200. [PubMed: 16430283]
45. Boudou T, Crouzier T, Ren KF, Blin G, Picart C. Multiple Functionalities of Polyelectrolyte Multilayer Films: New Biomedical Applications. Adv Mater. 2010; 22:441–467. [PubMed: 20217734]
46. Tang ZY, Wang Y, Podsiadlo P, Kotov NA. Biomedical applications of layer-by-layer assembly: From biomimetics to tissue engineering. Adv Mater. 2006; 18:3203–3224.
47. Lehaf AM, Moussallem MD, Schlenoff JB. Correlating the Compliance and Permeability of Photo-Cross-Linked Polyelectrolyte Multilayers. Langmuir. 2011; 27:4756–4763. [PubMed: 21443175]
48. Moussallem MD, Olenych SG, Scott SL, Keller TCS, Schlenoff JB. Smooth Muscle Cell Phenotype Modulation and Contraction on Native and Cross-Linked Polyelectrolyte Multilayers. Biomacromolecules. 2009; 10:3062–3068. [PubMed: 19817347]
49. Martinez JS, Lehaf AM, Schlenoff JB, Keller TCS. Cell Durotaxis on Polyelectrolyte Multilayers with Photogenerated Gradients of Modulus. Biomacromolecules. 2013; 14:1311–1320. [PubMed: 23505966]
50. Maloney JM, Walton EB, Bruce CM, Van Vliet KJ. Influence of finite thickness and stiffness on cellular adhesion-induced deformation of compliant substrata. Physical Review E: Statistical, Nonlinear, and Soft Matter Physics. 2008; 78
51. Martinez JS, Keller TCS, Schlenoff JB. Cytotoxicity of Free versus Multilayered Polyelectrolytes. Biomacromolecules. 2011; 12:4063–4070. [PubMed: 22026411]
52. Wallingford JB, Harland RM. Neural tube closure requires Dishevelled-dependent convergent extension of the midline. Development. 2002; 129:5815–5825. [PubMed: 12421719]
53. Ladoux B, Mège R-M, Trepat X. Front–Rear Polarization by Mechanical Cues: From Single Cells to Tissues. Trends in Cell Biology.
54. Mayor R, Etienne-Manneville S. The front and rear of collective cell migration. Nat Rev Mol Cell Biol. 2016; 17:97–109. [PubMed: 26726037]

Highlights

- Fish scale cell sheets migrate on PAH-PAABp polyelectrolyte multilayers.
- Sheets migrating on softer PEMUs periodically retract.
- Sheets durotax on modulus gradients.
- Myosin II inhibitors inhibit sheet integrity and migration.

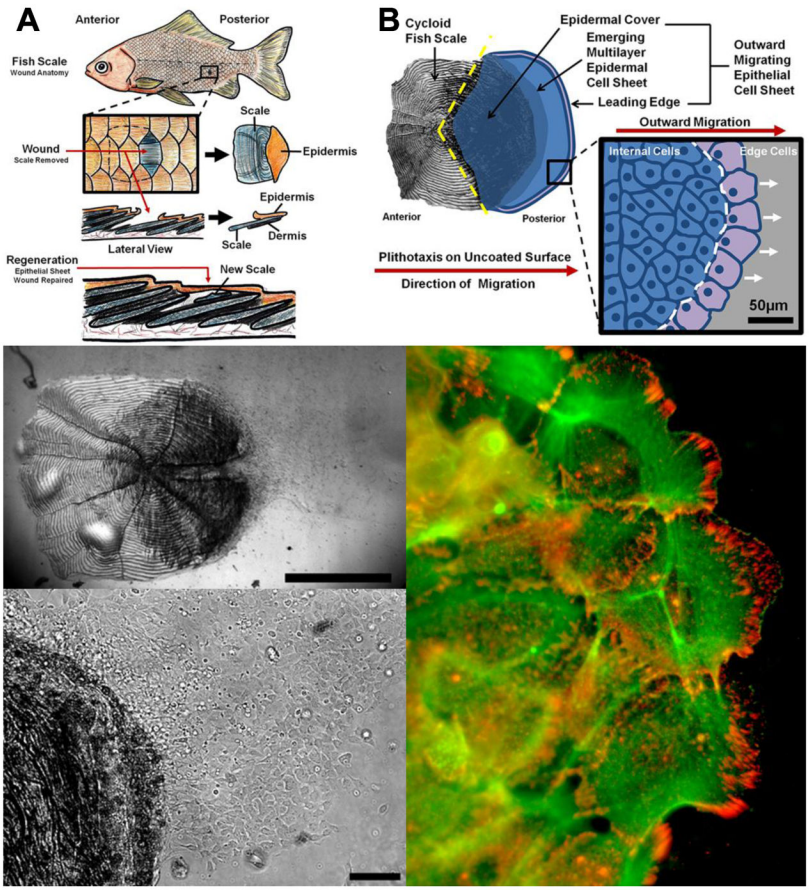

Fig. 1.

Epidermal cell sheet plithotaxis from an explanted cycloid (Comet Goldfish) fish scale. (A) Illustration of anatomical features of a cycloid fish scale showing scale removal for cell sheet investigation. (B) Diagram of an epidermal cell sheet composed of keratocytes, fibroblasts, and immune cells migrating from an explanted Comet Goldfish scale. The original anterior boundary of the epidermal sheet on the explanted scale is denoted by the yellow dashed line. The boxed area depicts intercellular interactions between sheet edge and internal cells, delineated by the dotted white line. (C and D) Phase contrast images of epidermal cell sheets emerging from fish scales of a Comet Goldfish. (E) Cells at the leading edge of a cell sheet migrating on an uncoated glass cover slip fluorescently stained for actin (green) and vinculin (red). Scale bars, (C) 1 mm; (D) 100 µm; E 20 µm.

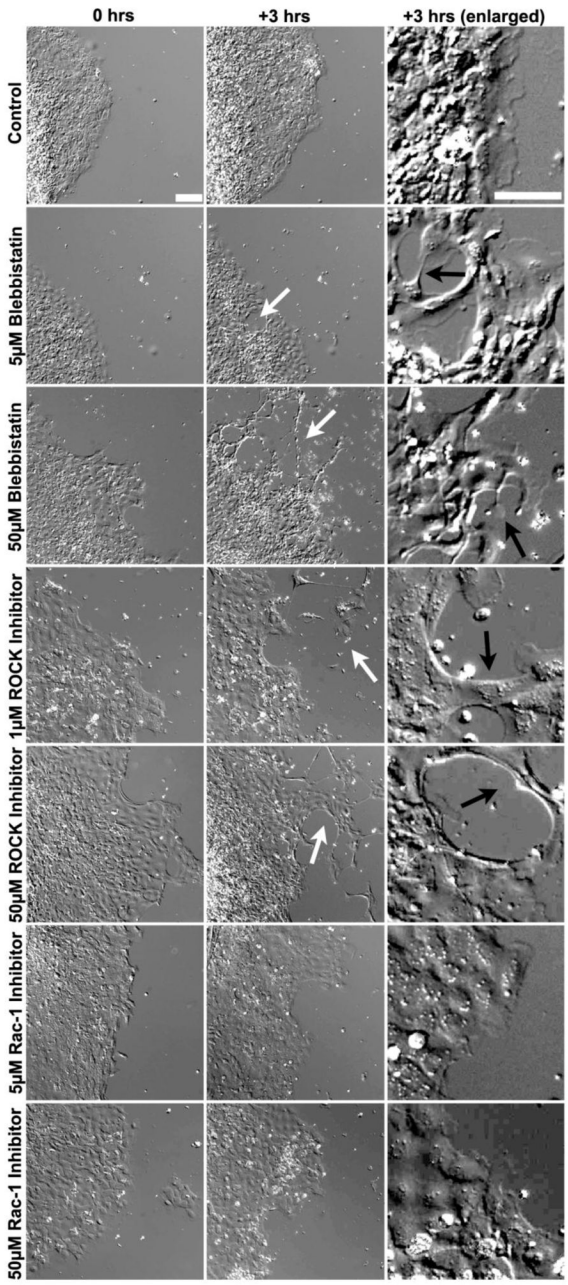

Fig. 2.

Myosin II-dependent cell sheet collective migration. Cell sheets migrating from explanted scales from a Comet Goldfish on uncoated glass coverslips were treated at 0 hr with 5 or 50 μM concentrations of the myosin II inhibitor Blebbistatin, the Rho kinase inhibitor Y27632, or the Rac1 inhibitor NSC23766. Arrows in the +3 hrs column indicate regions along leading edges of sheets where cell-cell junctions were disrupted after 3 hours of treatment in Blebbistatin or Y27632. Arrows in the +3 hrs (enlarged) column indicate regions along the magnified edge where cells exhibit abnormal motile morphology, in which the cell bodies appear overstretched. Scale bars, (0 and +3 hrs) 100 μm, (+ 3 hrs enlarged) 50 μm.

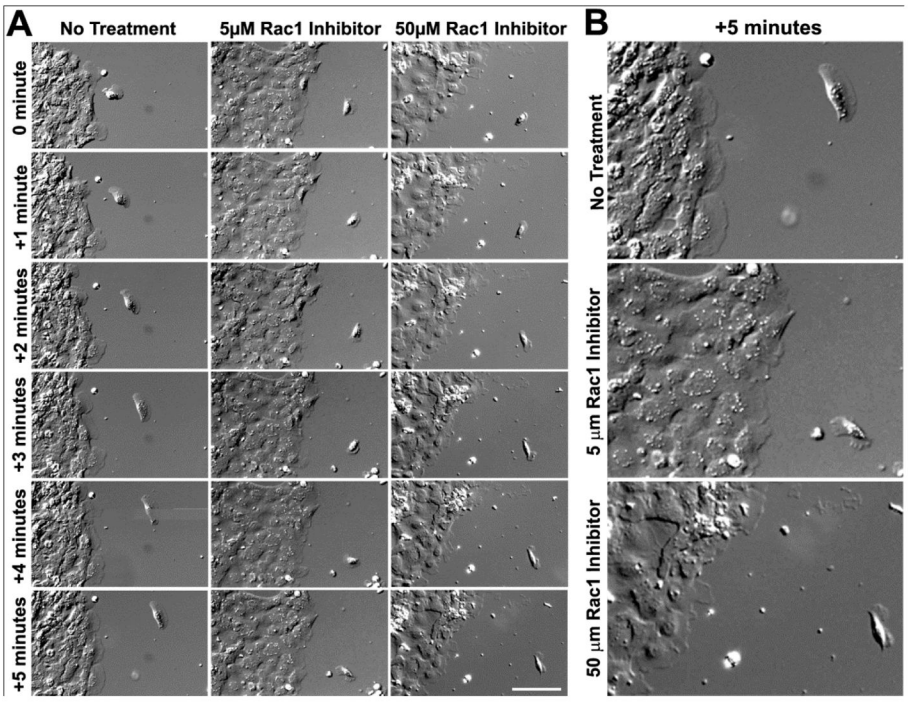

Fig. 3.

Rac-dependent lamellipodia ruffling. Epithelial sheet cells migrating from explanted Comet Goldfish scales on uncoated glass coverslips were treated with 5 or 50 μM concentrations of the Rac1 inhibitor NSC23766. (A, 0 minute row) Images were obtained 25 minutes after exposure to inhibitor and subsequent images were obtained at 1 minute intervals for 5 minutes thereafter. Scale bar, 100 μm. (B) Enlargements of cell sheet leading edge cell regions. (Supporting Information Fig S2 presents larger images of the single cells separated from the sheets.)

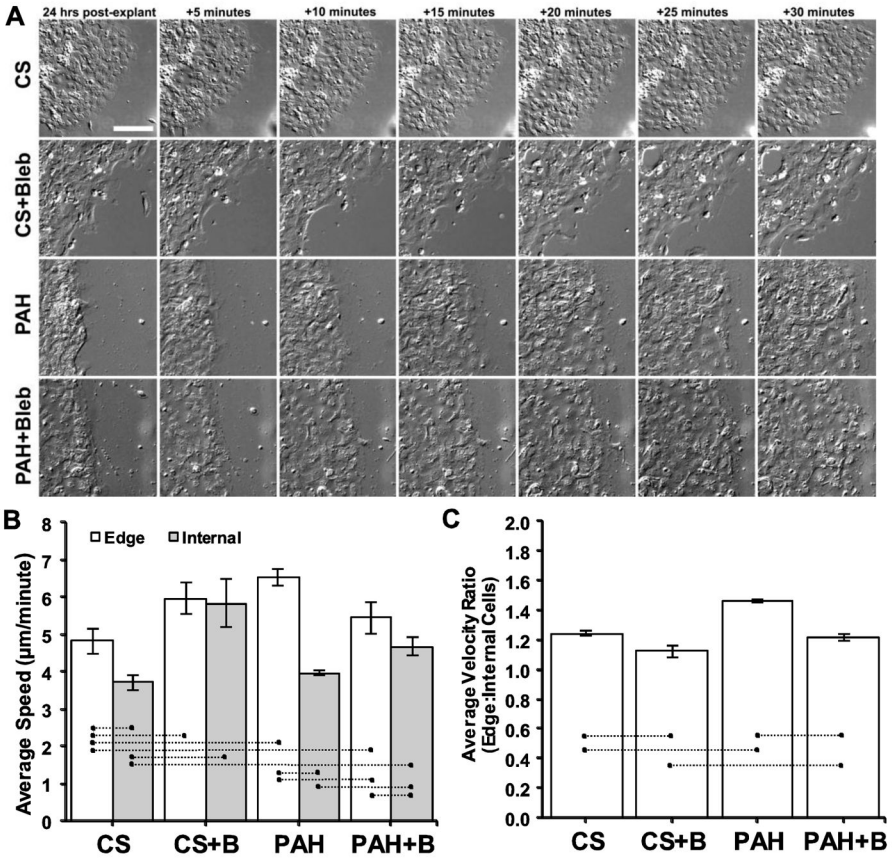

Fig. 4.

Myosin II inhibition reduces sheet cell migration velocity on PAH-PEMUs. (A) Epidermal cell sheets migrating from Black Molly scales on uncoated glass coverslips and on uncrosslinked PAH-PEMUs with uniform modulus (~38 MPa) were untreated or treated with the myosin II inhibitor Blebbistatin (5 μM) and imaged every 5 minutes for 30 minutes. (B) Migration velocities of edge and internal cells (n= 5 cells each) were measured as net distance of nucleus movement over 30 min in untreated and 5 μM Blebbistatin-treated sheets (+B) on coverslips (CS) and PAH-PEMUs (PAH). (C) Ratios of average edge to internal cell migration velocities. Dashed lines indicate Student's T-test P values of <0.05 for significance of difference between denoted conditions. Scale bar, 100 μm.

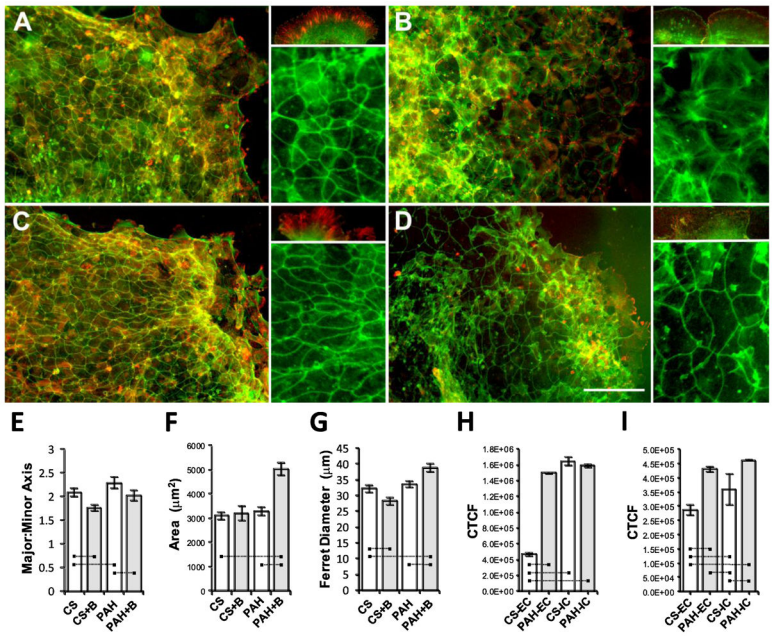

Fig. 5.

Myosin II inhibition in cell sheets on PAH-PEMUs reduces intercellular tension. Epidermal cell sheets migrating from Comet Goldfish scales on uncoated glass coverslips (A, B) and PAH-PEMUs (C, D) were untreated (A, C) or treated with 5 μM of the myosin II inhibitor Blebbistatin for 1 hour (B, D) and then fixed and fluorescently stained for actin (green) and vinculin (red). Insets are higher magnification images of edge cells from different sheets (top, red and green channels) and internal cells from the sheets shown (bottom, green channel only). Scale bar, 100 μm. (E) Average cell major to minor axis ratio, (F) average cell area, and (G) average feret diameter (cell length) for cells (n=50) from two trials were used to calculate values in E–G. (CS) uncoated coverslip, (PAH) PAH-PEMU, (+B) treated with 5 μM Blebbistatin. (H, I) Corrected total cell fluorescence (CTCF) of edge and internal cells in sheets migrating from Comet Goldfish scales on uncoated glass coverslips, “CS” (white) and PAH-PEMUs, “PAH” (gray) were stained for actin and vinculin. Dashed lines indicate Student’s T-test P values of <0.05 for significance of difference between denoted conditions.

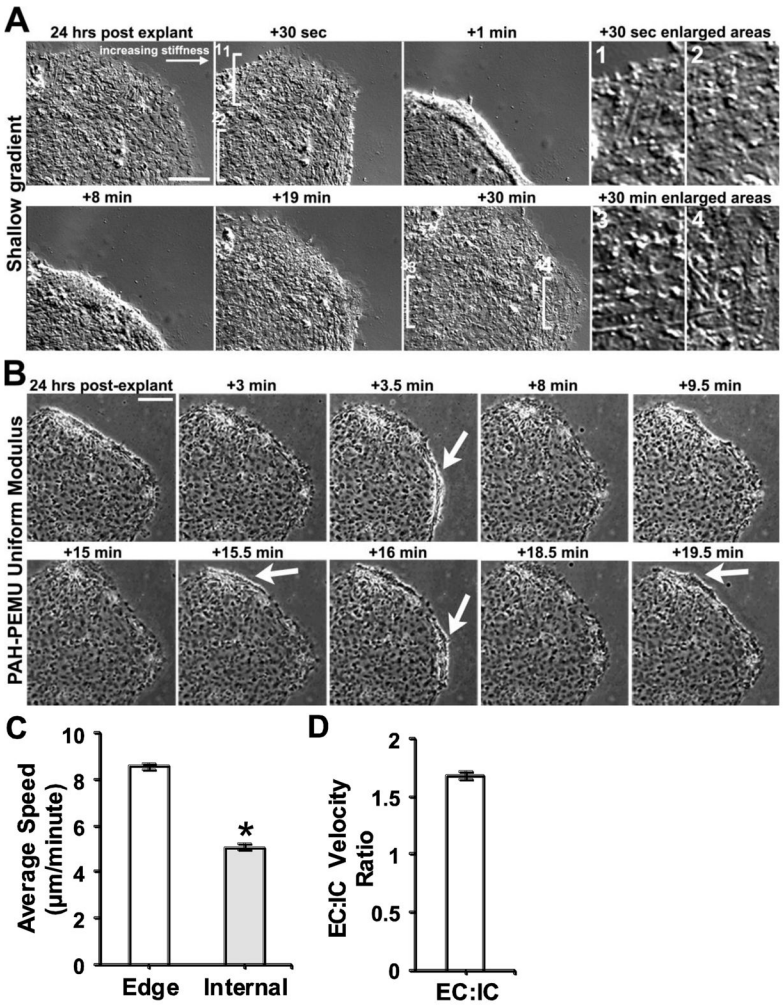

Fig. 6.

Epidermal cell sheet migration retractions on PAH-PEMUs. (A, B) Epidermal cell sheets migrating from Black Molly scales toward the stiffer end on the 90–120 MPa region of a shallow (~5 MPa mm^{-1}) modulus gradient and on a uniform modulus PAH-PEMU were imaged for the indicted times. (A, 1–4) Enlargements of indicated regions of a sheet migrating on a shallow gradient at the indicated times show linear elements indicating tension across the sheet along the directions of sheet migration. Arrows in (B) indicate regions of sheet retraction that are less extensive than the major retraction on the shallow modulus gradient in (A). (C, D) Migration velocities of edge and internal cells (n=5 cells each) on the shallow gradient were measured as net nucleus movement distance over 30 minutes. (D) Ratio of average edge cell to internal cell migration velocities on the shallow gradients. Asterisk indicates Student's T-test P values of <0.05 for significance of difference between denoted conditions. Scale bar, 100 μm.

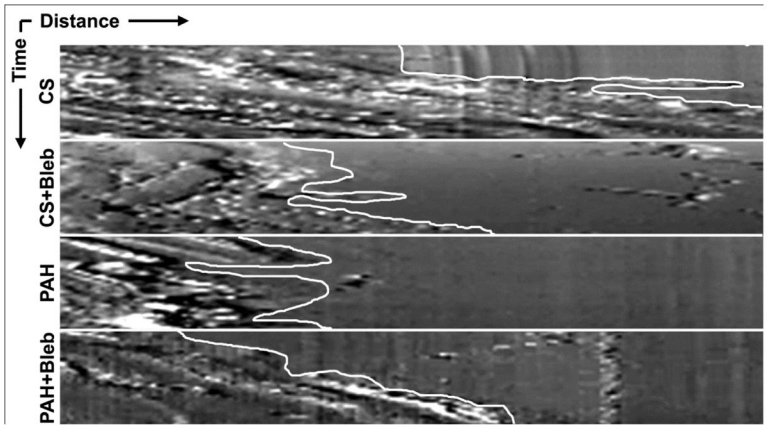

Fig. 7.

Myosin II-dependent retraction. Kymographs of cell sheets migrating for 30 minutes either untreated or treated with the myosin II inhibitor Blebbistatin on uncoated coverslips and on PAH-PEMUs of uniform modulus. Total distance shown is 350 μm.

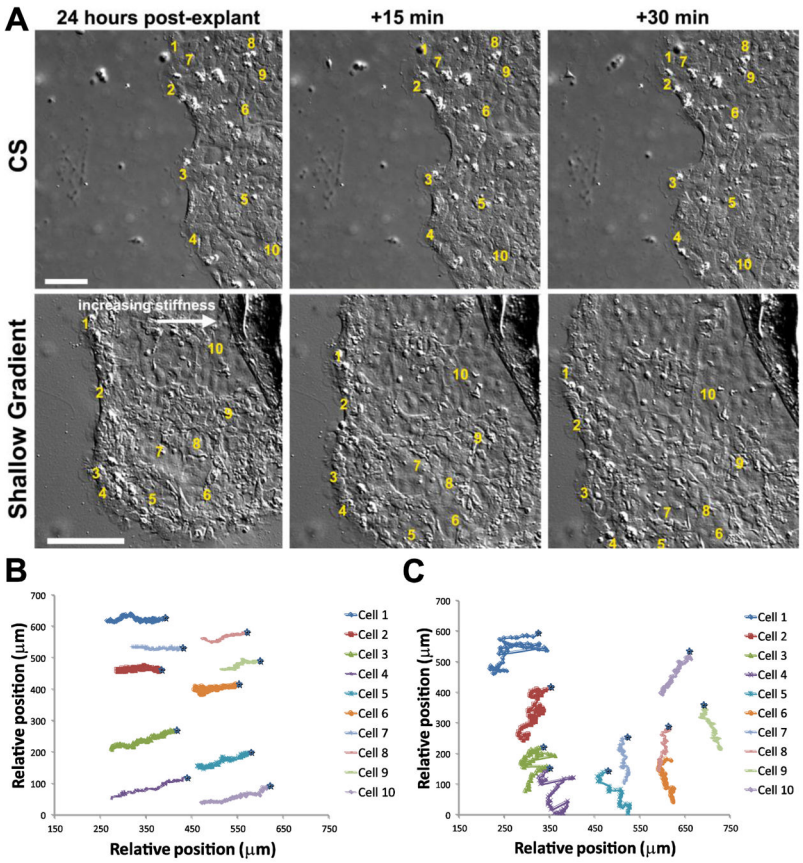

Fig. 8.

Epidermal sheet cells durotax on a PAH-PEMU shallow modulus gradient. (A) Epidermal cells sheets migrating from Comet Goldfish scales over a 30 minute period on an uncoated glass (CS) and oriented on a PAH-PEMU shallow modulus gradient with the direction of sheet emergence toward decreasing modulus (Shallow Gradient; arrow indicates direction of gradient). Relative positions and migration trajectory plots are mapped for 4 edge cells (1–4) and 6 internal cells (5–10) in the sheet on the uncoated glass coverslip (B) and in the sheet emerging toward the softer end of the shallow modulus gradient (C) with the starting position of each cell (*) and subsequent positions marked every 30 seconds. Scale bars, 100 μm.

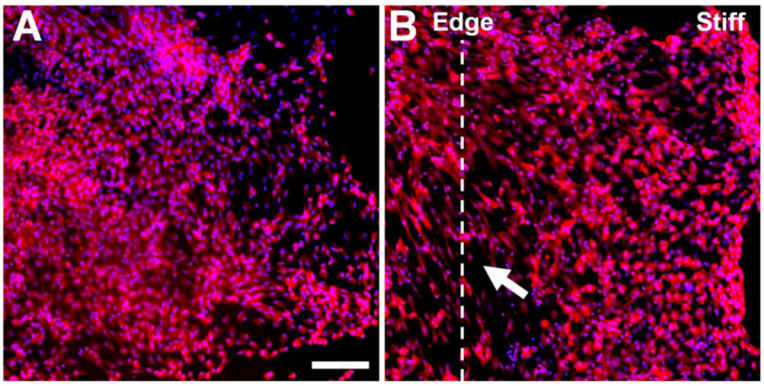

Fig. 9.

Epidermal sheet cells elongate and orient toward increasing stiffness on PAH-PEMUs with a steep modulus gradient. (A, B) Epithelial cell sheets emerging from Comet Goldfish scales placed on PAH-PEMUs of uniform modulus (A, ~120 MPa) and along a 0.65 mm region of a steep modulus gradient orient (B, ~1.5 mm; ~90 MPa to ~120 MPa, change of ~20 MPa/mm). Arrow indicates highly elongated cells over the region of the steep modulus gradient. Edge line indicates position of the mask used to generate the steep gradient. Cells were stained for actin (red) and DNA (blue). Scale bar, 100 μm.

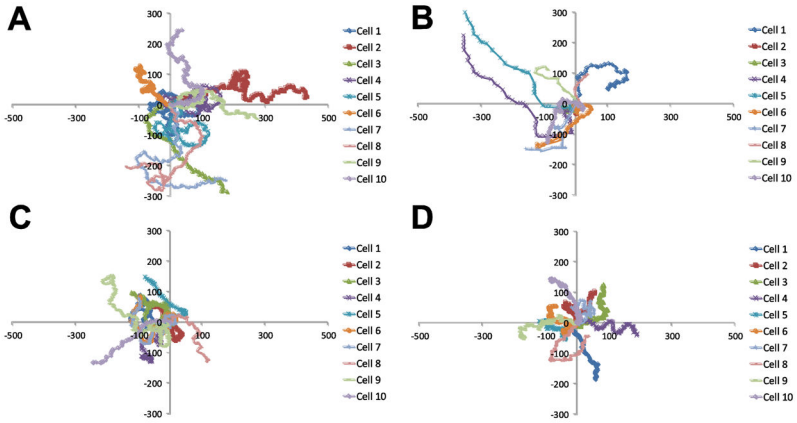

Fig. 10.

Individual keratocyte migration on PAH-PEMUs with shallow and steep modulus gradients. Explanted Comet Goldfish scales were placed on (A) an uncoated coverslip and PAH-PEMUs with (B) a uniform modulus (38 MPA), (C) a shallow modulus gradient (~15 mm, ~90 MPa to ~120 MPa), and (D) a steep modulus gradient (~1.5 mm; ~90 MPa to ~120 MPa) with the scale oriented so that sheet migration would initiate in a direction parallel to the modulus gradient and toward the stiffer end. Windrose plots were generated for the positions of the nucleus in individual cells (n=10) separated from each sheet and migrating independently of the sheet cells over 30 minutes.